

Single Event Effects in Avionics

Eugene Normand

*Boeing Defense & Space Group
Seattle, WA 98124-2499*

ABSTRACT

The occurrence of single event upset (SEU) in aircraft electronics has evolved from a series of interesting anecdotal incidents to accepted fact. A study completed in 1992 demonstrated that SEUs are real, that the measured in-flight rates correlate with the atmospheric neutron flux, and that the rates can be calculated using laboratory SEU data. Once avionics SEU was shown to be an actual effect, it had to be dealt with in avionics designs. The major concern is in random access memories, RAMs, both static (SRAMs) and dynamic (DRAMs), because these microelectronic devices contain the largest number of bits, but other parts, such as microprocessors, are also potentially susceptible to upset. In addition, other single event effects, specifically latchup and burnout, can also be induced by atmospheric neutrons.

I. INTRODUCTION

Over the last 10 years, the occurrence of single event upset (SEU) in aircraft electronics has evolved from a series of interesting anecdotal incidents [1] to accepted fact [2]. The anecdotal incidents had little scientific basis, relying exclusively on overall pilot observations, but they were a harbinger of things to come.

During 1988-89, IBM flew a series of proprietary flight experiments on three different aircraft in which upsets in a large array of 64K SRAMs were measured. A few years later, a joint IBM-Boeing study sponsored by DNA and NRL, collected the actual inflight upset data from both these IBM proprietary flights, and upsets recorded in the CC-2E flight computer on military aircraft. This study, completed in 1992 [3], demonstrated that SEUs in avionics are real, that the measured inflight rates correlate with the atmospheric neutron flux, and that the rates can be calculated using laboratory SEU data.

Once avionics SEU was shown to be an actual effect, it had to be dealt with in avionics designs. The major concern is in random access memories, RAMs, both static (SRAMs) and dynamic (DRAMs), because these microelectronic devices contain by far the largest number of bits susceptible to upset. The most common way of dealing with SEU in RAMs is by means of error detection and correction (EDAC); today a number of commercially available computer systems for upgrading military aircraft incorporate EDAC in their designs. This trend of building EDAC directly into the design is likely to continue as larger quantities of memory (from megabits to gigabits) are incorporated into avionics systems. In addition to upset, other single event effects (SEE, such as latchup and

burnout), although less probable, also pose potential concerns which can be dealt with in other specific ways, and these too will be addressed in this review.

II. THE ATMOSPHERIC ENVIRONMENT

The atmosphere is not nearly as benign as some might think, even with respect to the ionizing radiation environment. Therefore, in this section, the atmosphere will be described from the viewpoint of its ionizing radiation components; the experimental evidence for avionics SEU and effective SEU calculation methods will be presented in subsequent sections. For purposes of reviewing single event effects in avionics, the three main ionizing radiation components, neutrons, protons and heavy ions, will be described in some detail.

Modeling the Atmospheric Radiation Environment

For all of the ionizing particles within the atmosphere, the variation of the particle flux with three parameters is most important: energy, altitude and latitude. The energy variation is usually presented by plotting the differential flux (flux per unit energy) as a function of energy, which is often called the spectrum. The spatial variation is usually given as a function of altitude and latitude. However, geophysicists more accurately describe the variation with respect to two related parameters, atmospheric depth (in units of gm/cm²) instead of altitude, and vertical rigidity cutoff (in units of GV) instead of geographical latitude.

The atmospheric depth, x (gm/cm²), can be related to the altitude, A (feet), by the convenient relationship:

$$x = 1033 \exp\{-[0.4534 - (1.17 \times 10^{-9}) \times (A - 1.05 \times 10^5) / 1 \times 10^3]^{3.58}\} \times (A / 1 \times 10^3) \quad (1)$$

The latitude variation is expressed in terms of the vertical rigidity cutoff, R , in units of GV. [The rigidity of a charged particle of mass m , energy, E and charge q , is given by $R = (1/q) \sqrt{E^2 + 2mE}$.] The rigidity cutoffs are used to describe the strength of the earth's magnetic field which is strongest at the equator (requires particles with the highest rigidity, $R \sim 15$ GV, to penetrate to this region) and weakest at the poles (where particles with $R < 1$ GV can reach). The actual geographical distribution of the vertical rigidity cutoffs around the world have been given by Shea and Smart as isocurves on a world map [4]. To simplify the relationship between geographical latitude and rigidity cutoff, we averaged the Shea and Smart vertical cutoffs over geographical longitude for each 5° in geographical latitude. The resulting curve of averaged rigidity cutoff as a function of latitude has been presented in [5].

Neutrons

Atmospheric neutrons have been identified as the main cause of single event effects at elevated altitudes [2,3]. The neutrons in the atmosphere are created by the interaction of cosmic rays with the oxygen and nitrogen atoms in the air. They extend in energy to > 1000 MeV as can be seen in Fig. 1 which shows the differential neutron energy spectrum as measured by Hewitt et al, [6]. It has been found convenient to fit the spectrum of Fig. 1 as a function of neutron energy E

$$dN/dE = .3459E^{-.9219} \times \exp[-.01522(\ln E)^2] \text{ n/cm}^2\text{secMeV} \quad (2)$$

which applies at 40,000 feet and 45° latitude. Other researchers who have measured the atmospheric neutron spectrum obtained similar results, although in some cases the spectrum was found to reach a plateau at ~ 30-70 MeV before falling off as 1/E [7].

The neutrons in the atmosphere vary with both altitude and latitude. The altitude variation derives from the competition between the various production and removal processes that affect how the neutrons and the initiating cosmic rays interact with the atmosphere. The result is a maximum in the flux at about 60,000 feet, called the Pfotzer maximum as seen in Fig. 2 [2]. The 1-10 MeV neutron flux is often shown on a semi-log plot as a function of atmospheric depth [7] which is very similar to Fig. 2. Such a curve, which can be found in [6] or [8], more explicitly shows that at sea level (1033 gm/cm²) the neutron flux is several hundred times lower than at aircraft altitudes. Although the curve in Figure 2 is for only the 1-10 MeV neutrons, it is representative of the variation of the entire neutron spectrum. Normand and Baker have verified this by observing the same behavior of the 1-10 MeV and 10-100 MeV fluxes as a function of altitude. [5]

The latitude variation of the 1-10 MeV atmospheric neutron flux is shown in Fig. 3 [5]. Figure 3 is based on measurements made aboard aircraft at 35,000 feet [9], that were originally displayed as a function of vertical rigidity cutoff. The curve of averaged rigidity cutoff as a function of latitude was used to transform the original data into the form of Fig. 3, which is a simplified but yet very useful approximation for showing the variation of the atmospheric neutrons with latitude. In simplified terms, the atmospheric neutron flux appears to follow a form that combines both exponential and trigonometric behavior with latitude. The simplest such form, flux $\sim \exp[-\cos(2 * \text{Latitude})]$, gives the approximate shape, but a much better fit, in terms of L = latitude, is obtained using the following equation:

$$N_{1-10}(L) = 0.6252 \exp\{-.461 \times [\cos(2L)]^2 - .94 \times \cos(2L) + .252\} \text{ n/cm}^2\text{sec} \quad (3)$$

In combination, Figs. 1-3 define a simplified atmospheric neutron distribution model. It assumes that the neutron flux is separable into three factors, one that varies with altitude, one with geographical latitude and one to account for energy. A more accurate model, independent of the energy spectrum, is the Wilson-Nealy model [5,10]. In this model, latitude and altitude are not treated as separable factors, but rather are required to be expressed in terms of rigidity cutoff and atmospheric depth. In addition, this more refined model is very useful because it also accounts for the effect of solar modulation on the atmospheric neutron flux, which is generally a small effect.

Protons

Charged particles have also been measured in the atmosphere, most of which are, like the neutrons, reaction products from the interaction of the primary cosmic rays with the O and N nuclei in the air. These include protons, pions, kaons and electrons, with the pions and kaons decaying to muons. Most of the measurements were made on the ground at mountainous elevations (> 7000 feet), but these have been augmented by data from balloon measurements. Our interest is primarily on the protons because they can cause single event effects in a manner very similar to the neutrons.

Overall, the distribution of protons is similar to that of neutrons, especially with respect to energy and altitude. The energy spectrum of the atmospheric protons is similar to that of the neutrons, as seen in Figure 4, but it appears to have more peaks and valleys. Figure 4 contains the proton differential flux data from three sets of measurements, two at mountain tops (in the US by Barber [10] and in Russia by Kocharian [6]) and one from a Russian balloon experiment by Bogolomov [6]. The mountain top data are quite similar, with the higher altitude Russian data having a higher flux than that recorded by Barber in Arizona [10]. Both indicate a peaking in the differential proton flux at about 200-300 MeV. The balloon altitude proton fluxes of Bogolomov [6] appear to have the same behavior with energy as the mountain top data, although they do not cover as high an energy range. However, the magnitudes of the balloon proton fluxes are lower than might be expected, which may reflect a normalization problem. The balloon data are included to show that the proton spectrum remains relatively constant at all altitudes, as with the neutrons.

The proton flux falls off with altitude or equivalently, with atmospheric depth. This is seen in Figure 5 in which balloon measurements over Texas by Webber and McDonald [12], for proton energies in the 100-750 MeV range, have been combined with the integrated mountain-top data of Barber [11] shown in Figure 4. For these lower energy protons ($100 < E < 750$ MeV), the behavior is similar to that of the neutrons, i.e., there is a maximum at ~ 80 gm/cm² (55,000 ft.), the aforementioned Pfofzter maximum. The curve for 100-750 MeV proton in Figure 5 actually is quite similar to Figure 2 for neutrons. Just as the neutrons were shown to peak at $\sim 60,000$ ft, so too do the high energy proton flux measurements by McDonald and Webber ($E > 750$ MeV) show a maximum at between 50-100 gm/cm² (55,000 - 65,000 ft), the peak depending on the geomagnetic latitude [12].

Within the secondary protons, and in particular those having energies < 800 MeV, there are differences that are due to the distinct behavior of each of its two components. Those protons moving upward are called the "splash albedo" component, and those moving downward are called the re-entrant albedo component. The upward moving component is essentially constant with atmospheric depth, but the re-entrant component peaks at roughly 100 gm/cm². Because this reflects the peaking behavior previously discussed, it is therefore the dominant component [13].

A recent analysis [13] of these two components provides some insight into the latitude (or geomagnetic cutoff) variation of the atmospheric protons. At altitudes of interest, $\sim 40,000$ ft (200 gm/cm²) and for $E > 100$ MeV, the flux of vertically moving protons decreases monotonically with increasing geomagnetic cutoff (i.e., decreases monotonically in approaching the equator). The flux of downward moving protons however first increases and then decreases in traversing from polar to equatorial regions. The result is a slight decrease in the total atmospheric proton flux of about a factor of 2 in traversing from the polar to equatorial regions [13]. This is in marked contrast to the situation with neutrons for which the flux at the equator is lower by about a factor of 7 compared to that at the poles as seen in Figure 3.

Heavy Ions

Very few measurements have been made of the heavy ions in the atmosphere. The flux of the heavy ions within the primary cosmic rays is very rapidly attenuated with increasing atmospheric depth due to fragmentation (interactions with the atmosphere that fragment and thereby remove these heavy ions). Nuclear emulsion and plastic track

detectors have been used to measure the flux of enders, i.e., ions that are stopped within the detector. It was found that the flux of enders, incident from a specific zenith angle, is a function of the path length measured from the top of the atmosphere. Heavy ion fluxes as a function of the product of vertical atmospheric depth multiplied by the secant of the zenith angle have been measured for various ions groups and plotted and compiled by Fukui [7,8]. A similar set of curves of the vertical ion flux for four different ion groups is shown in Fig. 6 [14] which applies at the top of the atmosphere (0-80 gm/cm², equivalent to > 58,000 feet). Comparing Fig. 6 for heavy ions to Fig. 5 for protons shows how drastically the heavy ions are reduced by the atmosphere.

The data shown in Fig. 6 give no direct indication how the geomagnetic field, i.e., rigidity cutoffs, affect the heavy ion flux, although we would expect it to be somewhat similar to the effect on protons discussed above. More recent measurements were made on the aircraft flying the IBM avionics SEU experiment referred to in section III. CR-39 track etch detectors were flown on three flight paths: mid-latitude (low and high altitude) and high latitude, high altitude. Heavy ion strikes were measured on only the high latitude (polar), high altitude flight. The resulting linear energy transfer [LET, (dE/dx)/(density)] spectrum of these heavy ions has been plotted and is shown in [8]. For LET >1 MeV-cm²/mg, the atmospheric heavy ion spectrum appears to fall off precipitously and so it would not be expected to pose much of an SEE threat to avionics.

Future aircraft radiation environment programs may better define this heavy ion component. An ambitious program to measure all ionizing radiation components within the atmosphere at aircraft altitudes had been proposed by the DOE-EML [15]. It would have involved simultaneous measurements by about 10 different instruments aboard a single aircraft to record the neutron, proton and heavy ion particle fluxes and dose rate responses at different latitudes and altitudes. However, more recently organized flight measurement programs that are likely to be flown in the mid-1990s will not be as ambitious, but rather will concentrate on just neutron flux and dose rate measurements.

Aircraft Altitudes

Both the simplified model, Figs. 1, 2 and 3, and the more accurate Wilson-Nealy model, apply at all altitudes. With commercial air traffic, the altitude at which airplanes fly is a complicated matter based on many factors (weight of aircraft, fuel reserve requirements, air traffic control instructions, etc.). However, setting aside these limitations, there are default altitudes established by the ICAO (International Civil Aeronautical Organization) which are as follows: a) for eastbound flights - from sea level to 29,000 ft. at odd-numbered altitudes, and above 29,000 ft., at 33,000, 37,000, 41,000 and 45,000 ft. and b) for westbound flights - from sea level to 28,000 ft., at even-numbered altitudes, and above 28,000 ft., at 31,000, 35,000, 39,000 and 43,000 ft. The Concorde flies at about 55,000 feet and the next generation supersonic airplane, the HSCT (high speed civil transport) is being designed for a flight altitude in the range of 55,000 - 65,000 feet. For military aircraft that fly at distinctly different altitudes depending on the mission, determining a single flight altitude to characterize the neutron environment is not straightforward. An initial estimate can be made based on flight profiles in MIL-HDBK-781 [16]. For jet fighters on escort and operational missions, MIL-HDBK-781 gives 35,000 - 42,000 feet as the range of relevant altitudes, for electronic countermeasures and reconnaissance aircraft, it is 35,000 - 40,000 feet, and for

helicopters it gives 5000 feet as the altitude at which they fly from base to area of operation.

III. EXPERIMENTAL EVIDENCE

Inflight Upsets

SEU researchers had predicted that the neutrons and charged particles in the atmosphere would cause upsets in sensitive microelectronics devices as early as 1984 [17]. However, it was not until the 1991/2 IBM/Boeing study that the occurrence of single event upsets in SRAMs during flight was firmly documented [3]. In this study, upsets were recorded in 64K SRAMs flying at both 29,000 and 65,000 feet at a variety of latitudes, and when operated in both the standard 5V and 2.5V data retention modes. In all cases upsets were measured.

In the data retention mode, RAM boards were flown by IBM on close to 60 flights, accumulating nearly 300 flight hours and yielding about 75 upsets. Upsets were accumulated during each of three flight phases and read out at the end of each phase. Both the NASA ER-2 and Boeing E-3/AWACS aircraft were used. In the fully operational mode, data were collected from the CC-2E computer containing the same 64K SRAM, aboard military aircraft in two separate European areas. Because the CC-2E is protected by error detection and correction (EDAC), all upsets were detected, corrected and recorded by the computer for each flight. In this case there were 118 flights accounting for 783 flight hours which resulted in 136 upsets [2].

Since this initial study, two other papers have been published which further document in-flight SEU events. Normand and Baker reported on upsets in the CC-2E computer in the TS-3 Boeing E-3/AWACS that flies out of Boeing Field [5]. Its altitude is 29,000 feet but it flew to a variety of northern latitude locations, so upset data were obtained as a function of latitude for latitudes ranging from 30° to 60°. A total of 162 upsets was recorded in 130 flights, and 100 of these had latitude information available. J. Olsen et al., reported observation of 14 SEUs in the 256K SRAMs of a hand-held computer used in the cockpit of commercial aircraft flying at 39,000 feet [18].

Attributing the in-flight single event upsets to the atmospheric neutrons is based upon several factors. First, with the limited in-flight data available, Taber and Normand were able to plot the measured upset rates against altitude and latitude. These upset data were then correlated with the atmospheric neutron curves as functions of altitude and latitude and the agreement was good. Figure 7 shows the altitude variation [2] and Fig. 8 the latitude variation [5]. Because the in-flight upset rates as functions of altitude and latitude directly follow the variation of the atmospheric neutron flux with the same variables, it is clear that the atmospheric neutrons are the dominant radiation environment influencing the upset rate. Table 1 lists most of the known instances of SEU experienced in avionics. Also included in the table are the SEU rates calculated by one of two different methods discussed in section IV. The good agreement between these calculated rates listed in the last column (obtained using the atmospheric neutron flux combined with SEU cross section data) and the inflight measured rates also supports the idea that it is the neutrons that are responsible for the upsets.

The ease by which upsets can be measured during flight depends on the system being used. There are at least three approaches with some variations: the first two, EDAC and parity/dual redundancy, apply during flight; the third, comparison of pre- and post-flight bit patterns does not. In systems employing EDAC, the contents of the entire

memory are continuously scanned so that errors are detected, corrected and logged [2]. In systems using simple parity or dual redundancy schemes to ensure system integrity, upsets are less certain because only errors occurring between write and subsequent read portions of the system cycle are detectable. Thus the actual upset rate may be underestimated unless the fraction of flight time during which the RAM errors are capable of being detected can be estimated based on system operation. For flight experiments the third method can be used as with the IBM tests. RAM parts were initialized, operated in standby mode for some number of flights, and read out afterwards in normal mode, the comparison against the initial pattern indicating how many upsets had occurred.

Table 1. Measured In-Flight Occurrences of Avionics Single Event Upset (SEU)

Aircraft/ Reference	Flight Path	Alti- tude K ft	Opera- ting Voltage	Electronic Part	Measured Rate, up/bit hr	Calculated Rate,* up/bit hr
E-3/[2]	Seattle	29	2.5 V standby	IMS 64K SRAM	5×10^{-9}	$4.4-8 \times 10^{-9}$
ER-2/[2]	N. Cali- fornia	65	2.5 V standby	IMS 64K SRAM	1.1×10^{-8}	$1-2 \times 10^{-9}$
ER-2/[2]	Norway	65	2.5 V standby	IMS 64K SRAM	2.3×10^{-8}	$2-4 \times 10^{-8}$
ER-2/[2]	Norway	65	2.5 V standby	EDI 256K SRAM	4.6×10^{-9}	$8-14 \times 10^{-9}$
Similar to E-3/[2]	Europe Area 1	29	5 V	IMS 64K SRAM	2.3×10^{-9}	$1.8-4.7 \times 10^{-9}$
Similar to E-3/[2]	Europe Area 2	29	5 V	IMS 64K SRAM	1.6×10^{-9}	$1.3-2.7 \times 10^{-9}$
E-3/[7]	Out of Seattle	29	5 V	IMS 64K SRAM	1.6×10^{-9}	$1.3-2.7 \times 10^{-9}$
Com'cl Jetliner/[16]	Trans- Atlantic	~35	5 V	EDI 256K SRAM	2×10^{-9}	1×10^{-9}
Fleet of Com'l Jets/ [19, 20]	World- wide	~25 -33	5 V	IDT 256K SRAM	3.3×10^{-10} , 4.1×10^{-10} (used by 2 dif- ferent avionics vendors)	5×10^{-10}

* Calculated rates are given as either a single value, in which case the rate is from the Burst Generation Rate (BGR) method, or as a-b, where a is the rate from the neutron cross section method, and b is from the BGR method.

Charge Collection Measurements

A second confirmation of the primary role of the atmospheric neutrons is offered by the energy deposition measurements made by the CREAM instrument aboard the Concorde. [21, 22] CREAM was originally developed to measure the energy deposition spectra in silicon on the Shuttle. It consists of ten pin diode detectors operated at 172

μm of depletion and with a total sensitive area of 10 cm^2 . It was installed and flown on the Concorde supersonic aircraft in 1988 and data were recorded from 1988-90 at altitudes above 50,000 feet. Energy deposition is collected in 9 separate channels, but on all flights the two highest channels never recorded any counts. Across the seven lower channels the count rates were remarkably similar for such flight paths as London-New York, London-Washington and Washington-Miami. The count rate data were converted into the burst generation rate format, $\text{cm}^2/\mu\text{m}^3$, and these are shown in Fig. 9.

Normand et al. recently performed a charge collection experiment at the Weapons Neutron Research (WNR) facility at Los Alamos National Laboratory [23]. The spectrum of the WNR neutron beam shown in Fig. 10 is very similar to that of the atmosphere (Fig. 1) except it is approximately 1.5×10^5 times more intense [23]. A silicon surface barrier detector (300 μm fully depleted) was exposed to the WNR neutron beam and the energy deposition spectrum measured [23]. This too is shown in Fig. 9 and it is evident that the CREAM data measured in flight parallels the neutron bombardment energy deposition. The WNR deposition spectrum is higher because the depletion depth of our detector is larger than that of the CREAM detectors (300 μm vs. 172 μm). Figure 9 also shows that about 120 MeV is the maximum energy that can be deposited by atmospheric neutrons. This is consistent with the CREAM data since no counts were recorded in channel 8 (182 MeV).

Ground Level Upsets

The neutron environment at ground level can also be defined using Figs. 1-3, or the more accurate Wilson-Nealy model, with the recognition that the elevation of a particular location above sea level needs to be specified. Limited data from a sophisticated ground-based detector system made at 100, 5000 and 10,000 feet above sea level indicate that the 10-100 MeV flux falls off approximately linearly with elevation [5]. Very few measurements of the neutron spectrum at ground level have been made, especially over the entire energy range. One set of the most recent measurements, made in Japan [24], was normalized to the spectrum expected in the US based on airplane measurements over Japan [24] and the US [6]. These spectra are found in [8] and show that the ground spectrum is roughly 1/300 of that at 40,000 ft.

An early study showed that when a large number of memories was monitored for single event upset at three locations of varying altitude (5000 feet, sea level and in a mine), the upset rate decreased with decreasing elevation, indicating that atmospheric neutrons are the likely cause [25]. This study has been recently published in a much updated format [26] that carefully separates out the upsets caused by alpha particles emitted by trace elements in the device package from those caused by the atmospheric neutrons. Using the atmospheric upset rate component at three locations within the US, the variation with altitude is the same as the atmospheric neutron flux variation with altitude [23].

There is even more recent evidence of upsets on the ground. The large computer system ACPMAPS at Fermilab contains about 160 Gbits of DRAM memory, which, when fully monitored, exhibited approximately 2.5 upset/day [27], equivalent to $\sim 7 \times 10^{-13}$ upset/bit-hr. This upset rate appears to be consistent to within about a factor of 2-3 with the rate calculated using the ground level neutron flux (1/300 of Fig. 1), combined with a measured DRAM upset rate in the WNR neutron beam [23]. Further, RAM manufacturers perform quality control soft error rate (SER) tests at their facilities in

which they look for bit errors when monitoring 1000 parts for 1000 hours, the error rate being given in FIT units, defined as errors per 10^9 device hours (failures in time). Lage showed [28] that for current RAMs, FIT rates are typically in the range of 600-5000 FITs for 256K, 1M and 4Mbit devices. These FIT rates are equivalent to approximately 10^{-12} upset/bit-hr (there is some ambiguity regarding which FIT rates apply to which size devices). This is very similar to the rate measured at Fermilab, and is a rate that can be attributed to the atmospheric neutrons based on the WNR test data indicated above, as well as calculations with the BGR method [23].

Some have speculated that at ground level pions make the largest contribution to SEUs in memories. The relatively good correlation cited above between the measured ground level SEU rates with the calculated rates based on neutrons at ground level appears to contradict this idea, indicating that neutrons play the major role. Pions may contribute to some portion of the SEU rate at ground level, but it appears that the atmospheric neutrons are mainly responsible for ground level upsets. In the future, when parts may have much smaller ($\sim 0.1 \mu\text{m}$) feature sizes, pions may play a larger role.

IV. CALCULATIONAL APPROACHES

Using Neutron/Proton SEE Data

In the original IBM/Boeing study, the authors offered two methods for calculating avionics SEU rates, one that uses the neutron/proton SEU cross section, $\sigma_{\text{nseu}}(E)$, and one that uses heavy ion SEU cross sections. The first method, the neutron cross section (NCS) method, is straightforward. It gives the rate as the integral over neutron energy of the differential neutron flux multiplied by the neutron SEU cross section.

$$\text{Upset rate} = \int \sigma_{\text{nseu}}(E) (dN/dE) dE \quad (4)$$

where

$$\begin{aligned} \sigma_{\text{nseu}}(E) &= \text{Neutron-induced SEU cross section} \\ (dN/dE) &= \text{Atmospheric differential neutron flux} \end{aligned}$$

The main drawback is that there are very few neutron SEU cross sections that have been measured. The reason for this is the lack of monoenergetic neutrons sources at a variety of neutron energies. The 14 MeV neutron generator does produce neutrons that are essentially monoenergetic, but it is at a single, relatively low energy. SEU cross sections for 14 MeV neutrons have been reported for several devices [2,8]. Pseudo-monoenergetic neutron sources, such as those using the Li(p,n) reaction, are available, but they have to be used with caution because there are very roughly as many neutrons in the peak (i.e., at E_{peak}) as there are in the tail portion of the spectrum that extends from $(E_{\text{peak}}-2)$ MeV down to 1-5 MeV [30].

There is an alternative, and that is to use the proton SEU cross section as the neutron SEU cross section. This holds for $E > 100$ MeV, and there is a larger number of proton SEU cross sections in the literature than neutron cross sections. This is the case because: a) the proton environment is important for low earth orbit satellites and b) many monoenergetic proton beams are available around the world that have been used for SEU testing (Harvard Cyclotron, UC Davis Cyclotron, LAMPF, Saturne, TRIUMF, etc.)

In addition to being straightforward, the NCS method of Eq (4) offers the advantage that, when it has been applied to proton-induced SEU in spacecraft, the

measured upset rates have been in good agreement with the calculated rates [8]. When this method was applied to the in-flight upsets in the 64k SRAM of the CC-2E, good agreement was again achieved with the calculated rate, as seen in Table 1.

Using Heavy Ion SEE Data

A number of microelectronic devices have been tested for SEU with protons, but at least ten times that number have heavy ion SEU data available. The heavy ion data have been obtained to support the evaluation of SEU rates caused by cosmic rays in parts intended for space applications. However, this data can also be used via the Burst Generation Rate (BGR) method to calculate SEU rates due to neutrons or protons.

The BGR method was first put forth by Ziegler and Lanford [31] and further refined for neutrons in [32]. In this method, all the energy deposited in the sensitive volume of a microelectronic device that leads to upset is assumed to be from the recoils resulting from neutrons reacting with the silicon. The recoils have low energies (<20 MeV) and therefore have ranges of a few micrometers in silicon so that almost all of this energy can be deposited within the device sensitive volume.

Thus, neutrons cause SEU not through direct ionization, but rather through nuclear reactions with the silicon resulting in recoils that can deposit enough energy in the sensitive volume to generate an upset. The burst generation rate function, $BGR(E_n, E_r)$, quantifies this in terms of the probability that a neutron of energy E_n will generate recoils with energy $\geq E_r$ in the silicon. Thus, for a given deposition energy, E_r , the deposition rate due to a flux of neutrons of energy E_n , $\phi(E_n)$, in the sensitive volume V is given by $C VBGR(E_n, E_r) \phi(E_n)$ where C is the collection efficiency that accounts for not all of the recoil energy being deposited within V . BGR functions for neutrons, in units of $cm^2/\mu m^3 \times 10^{-16}$, have been calculated using basic nuclear interaction data [32-34].

The BGR method has been refined to enable full use to be made of the information contained in the heavy ion cross section vs. LET curve by viewing a device as a population of cells. Each cell will upset when an amount of energy, characterized by an effective LET, is deposited in that cell. All cells are different, and the heavy ion cross section curve is really the integral over all cells in a device, showing the distribution of the probability to collect charge as a function of the critical charge [35].

The heavy ion SEU cross section, $\sigma(L)$, is generally plotted as a function of the LET of the ion [35]. It has been found to be most convenient to fit a smooth curve to the upset cross section as a function of LET, and the form of the fit most favored by a group of SEU experts is that of the Weibull distribution [35] given by:

$$\sigma(L) = \sigma_0 \{1 - \exp\{-(L - L_0)/W\}^S\} \quad (5)$$

where σ_0 is the asymptotic cross section

L_0 is the LET cutoff

S and W are fitting parameters

Generally a least squares fitting method is applied to obtain the Weibull parameters. Examples of the efficacy of the Weibull distribution to fit SEU cross section data are shown in [8,35].

To implement the BGR method, the heavy ion cross section curve, given by the Weibull fit [Eq. (5)], is divided into LET intervals, each representing a different energy deposition, and normalized by the corresponding SEU cross section over that interval.

The contribution by neutrons to each energy deposition interval is given [5] in terms of the BGR as follows:

$$\text{Upset Rate} = C \sum_i \Delta V_i \int_E \text{BGR}(E, E_{ri}) (dJ/dE) dE \quad (6)$$

where

- C = collection efficiency
- ΔV_i = ith sensitive volume
- E_{ri} = ith recoil energy, MeV
- BGR(E, E_{ri}) = burst generation rate, $\text{cm}^2/\mu\text{m}^3$, probability that particle of energy E will produce recoils of energy $\geq E_{ri}$
- dJ/dE = neutron/proton differential flux

$$\Delta V_i = t \Delta \sigma_i, \mu\text{m}^3 \quad (7)$$

where

- t = sensitive thickness, μm
- $\Delta \sigma_i$ = $\sigma_i - \sigma_{i-1}$
- σ_i = heavy ion SEU cross section for ith portion of the curve obtained using the Weibull distribution, cm^2

$$E_{ri} = t \times 0.23 \times \text{LET}_i, \text{MeV} \quad (8)$$

where

- t = sensitive thickness, μm
- LET_i = representative LET for ith portion of the curve, MeVcm^2/mg

An additional parameter implicit in Eq (6) but explicit in Eqs (7) and (8) and required in the neutron/proton SEU method, is the collection depth, t, sometimes called the sensitive thickness. The sensitive thickness can be considered as comprised of three parts: the depletion region, a funnel region and a diffusion region, with the depletion region generally the largest contributor [36]. Without any other information, $t = 1\mu\text{m}$ is sometimes used for the thickness, although this is conservative and leads to overestimating the upset rate. For recent parts, t has been seen to vary from 1-6 μm , with most parts having values in the range of 2-5 μm [35]. Based on our experience in using the method, we find that for parts fabricated in the 1990s (e.g., SRAMs of 256 Kbits or larger) a value of $t=2\mu\text{m}$ works well, for parts from the early-middle 1980s, a value of $t=5\mu\text{m}$ works well, and for parts in between, the best value of t lies between 2-5 μm . For the second parameter, C, the collection efficiency, it has been found that a value of $C \sim 0.5$ leads to good agreement between calculated and observed SEU rates and cross sections, when used in conjunction with the aforementioned values of t.

While it may appear to be an oversimplification to use a single value of t in the BGR method for a variety of microelectronic devices, the method does work. It appears that the main reason for this is that the calculations are carried out on a per bit basis, and at this level, the recoils do contribute most of the energy collected by the logic cell of a device, resulting in an upset. The success of the method has been borne out through two distinctly different sets of comparisons. The first is by comparing the calculated atmospheric neutron upset rates against the measured in-flight rates as shown in Table 1.

The second is by recognizing that the BGR method can also be applied to obtain neutron/proton-induced SEU cross sections, $\sigma(E_p)$, at neutron/proton energy E_p . This relies on two factors: 1) calculated BGR functions for both protons and neutrons are very similar and can be used essentially interchangeably, and 2) if the flux term, dJ/dE , in Eq. 6 is deleted and the integration over E removed, the equation gives the proton/neutron SEU cross section (cm^2/bit) rather than the SEU rate (upset/bit-hr). Thus $\sigma(E_p)$ is given as:

$$\sigma(E_p) = C \sum_i \text{BGR}(E_p, E_{Ti}) t \Delta\sigma_i \quad (9)$$

When this method was applied to two sets of data (measured heavy ion and proton SEU cross sections) for three different 64K SRAMs, the calculated proton SEU cross sections were in fair to good agreement with the measured data over the proton energy range of 50-500 MeV [37]. In addition, when the method was applied to measured SEU cross sections from 14 MeV neutrons in a variety of RAMs, again good agreement was obtained.

V. SIMULATION AND TESTING

As indicated above, there are very few monoenergetic neutron sources available that can be used to test microelectronics for their susceptibility to SEE. The available choices are really that of the 14 MeV neutron generator and proton beams with $E_p > 100$ MeV which have essentially the same effect as neutrons of the same high energies. Although pseudo-monoenergetic neutron sources, especially the Li(P,n) sources appear to be attractive because of availability and high neutron energies, that is offset by the need to distinguish between the upsets caused by the neutrons in the tail portion of the spectrum, compared to those due to neutrons in the peak. The BGR method has been used to distinguish between the two contributions by means of a calculated peak-to-total-spectrum adjustment factor [3], but it has received limited use. Another easily available source, the isotope PuBe, has also been used in some studies [8,38], but it produces only low energy (< 10 MeV) neutrons.

However, there is a much better alternative and that is a spallation neutron source which has a very similar spectrum to that of the atmospheric neutrons. Undoubtedly the best spallation source for SEU testing is the Weapons Neutron Research (WNR) facility at Los Alamos National Laboratory [39]. As shown in Fig. 10, the WNR neutron energy spectrum is very close to that of the atmospheric neutrons, but it is about a factor of $\sim 2 \times 10^5$ more intense. Thus, one hour in the WNR beam is the equivalent of roughly 2×10^5 hours at 40,000 ft altitude. A large test chamber and associated data acquisition trailer have been set up along beam line 30L to support SEE testing. The neutron spectrum is continuously being measured by means of a fission ionization detector system. The disadvantages of WNR are that a) it only operates once a year for a period of 2-4 months (varies from year to year), and b) to gain access to the beam, a user must gain approval of the Neutron Program Advisory Committee (NPAC).

There are other spallation sources having close to the right spectrum, but they are less convenient than the WNR for purposes of performing SEU testing. These sources are areas around a very high energy accelerator where the shielding is thinner than usual (by design or by accident) so that a higher neutron flux is present. Probably the best of these is the Reference Field Facility sponsored by the Commission of European Communities

(CEC) at CERN mainly for purposes of assessing the radiation exposure of civil aviation crews [40]. Other sources include the TNF (thermal neutron facility) at TRIUMF [8, 41] and the "soft reference field" (in the labyrinth) and "hard reference field" (behind the target room) areas of the phasotron at the Joint Institute of Nuclear Research, Dubna, Russia [42]. In all these cases, the neutron flux is higher than that of the atmospheric neutrons, but by only 1-2 orders of magnitude, not nearly as large as the factor of 2×10^5 at WNR. Furthermore, compared to the WNR, these accelerator sites don't have a means for continuously monitoring the spectrum of the neutron beam, nor do they provide convenient services for setting up equipment to carry out single event testing.

VI. OTHER SINGLE EVENT EFFECTS

Latchup

The high energy atmospheric neutrons may also induce other single event effects. The effect that has been measured in simulation with both the WNR beam [43, 44] and proton beams [45, 46] is latchup. Only a small number of parts has been found to be prone to neutron/proton-induced latchup. Included are specific memories [45, 47], a number of microprocessors [46, 48] and two specific types of gate arrays [43, 44]. From all data that are available, it appears that parts that undergo heavy ion-induced latchup will also be prone to neutron/proton latchup if the LET threshold for latchup is $< 5 \text{ MeVcm}^2/\text{mg}$. This is not a firm criterion but rather an approximate guideline. The key point is that based on the WNR testing [43, 44], the latchup rate is much lower on a per device basis, than the upset rate. If the upset rate is roughly 10^{-9} upset/bit hour (typical of at least five RAMs [8,23]), a 1 M bit RAM will have a per device SEU rate of 10^{-3} upset/device-hr. Worst case neutron/proton-induced latchup rates appear to be in the range $10^{-6} - 10^{-7}$ latchup/device hr [43-48].

The use of simple models based on only energy deposition to predict the neutron/proton induced latchup rate does not appear to work as well as it does for upset. They appear to be overly conservative, in effect, too much energy is deposited resulting in a calculated latchup rate that is ~two orders of magnitude too high. At present two more elaborate models for neutron/proton induced latchup have been published [44, 47] that improve on simple energy deposition as the only criterion. One is based on track electric field reduction of the LET of the recoils [47], but the tools to implement it are not readily available. The second model is based on a minimal required range for the recoils and has the following elements: a) it incorporates geometric factors that are based on standard microelectronics design practices, as well as on some preliminary specialized heavy ion latchup test results, b) it uses the general BGR methodology but for smaller sensitive volumes, and c) it uses heavy ion latchup cross section data [44]. Both of these models have given good agreement with measured neutron and proton induced latchup rates. As this issue receives further attention, it can be expected that additional models may be developed for calculating this effect.

Burnout

It is well known that when heavy ions of relatively high LET ($>20 \text{ MeVcm}^2/\text{mg}$) strike an N-channel power MOSFET, the energy deposited can lead to one of two single event effects (SEE), burnout or gate rupture [49]. Burnout is an effect that has also been induced by energetic protons [50], neutrons [51] and low LET ($<10 \text{ MeVcm}^2/\text{mg}$) heavy

ions [52], but gate rupture has not. In single event burnout (SEBO), the energy deposited by an energetic particle can forward bias the thin body region under the source. If the bias applied to the drain exceeds the local breakdown voltage, the single event induced pulse can initiate avalanching in the drain depletion region. Local power dissipation due to the large drain-source current leads to destructive burnout.

Most SEBO testing of N-channel MOSFETs has been conducted with ions having high LETs (i.e. high stopping power, $> 26 \text{ MeVcm}^2/\text{mg}$). The objective of this testing is to determine, for an ion of a given LET, what is the lowest drain-source voltage (V_{DS}) that will induce SEBO. Test methods were developed for conducting the burnout testing without destroying the parts and measuring individual burnout pulses [52]. A few tests were also conducted with low LET ions as well [52]. These showed that, in some parts, if V_{DS} is high enough but still less than the rated breakdown voltage, even low LET ions ($< 10 \text{ MeVcm}^2/\text{mg}$) can cause burnout. If low LET ions can cause SEBO then it is possible for the recoils induced by high energy neutrons/protons in the silicon to also cause burnout.

In the only previously published study in which power MOSFETs were exposed to energetic protons, the 100 V rated parts showed no SEBO but the 200V parts did [50]. In that case the SEBO testing with protons showed that at very close to rated voltage, N-channel power MOSFETs had a cross section for inducing SEBO of $\sim 10^{-9} \text{ cm}^2$, however this was reduced significantly when V_{DS} was lowered by as little as 10V.

It is known from testing with heavy ions [53] that the higher the rated voltage, the smaller the fraction (minimum V_{DS} at burnout)/(rated voltage) at which the parts exhibit SEBO. Thus it appeared that high voltage parts (e.g., 400V and 500V) would have a higher potential to experience SEBO due to protons and neutrons than lower voltage parts. This was confirmed in very recent Boeing tests with 400V and 500V MOSFETs in the WNR neutron beam [51]. Neutron-induced burnout was measured in these devices when V_{DS} was $> 300\text{V}$, and the cross section increased from $\sim 10^{-10} \text{ cm}^2$ to $\sim 10^{-7}\text{-}10^{-8} \text{ cm}^2$, as V_{DS} increased from 300 to 400V. However, since in current avionics applications these parts are operated at voltages lower than 300V, it appears that SEBO is not a real issue for current avionics.

Effects in Fiber Optic Systems

Photodiodes are used within the receiver portion of fiber optic data systems, and their sensitivity to ionizing radiation, in particular to single event effects (SEE) has been shown since the early 1990s [54, 55]. SEE testing of fiber optic systems demonstrated that both Si and InGaAs photodiodes are the most sensitive components [54]. The photodiodes have been tested with proton beams and measured in terms of the induced bit error rate [54, 55]. Since the bit error rate has been observed to increase with decreasing proton energy, the main mechanism identified is that of direct ionization energy loss rather than proton-induced nuclear interaction [55, 56].

More recently the WNR neutron beam was used to directly measure the sensitivity of InGaAs photodiodes to nuclear induced effects [57]. Using a 1000 μm diameter InGaAs photodiode, roughly 4×10^6 pulses were recorded for a neutron fluence of $\sim 3 \times 10^{10} \text{ n/cm}^2$, or about one pulse per 10^4 particle/cm². With protons, essentially every particle leads to a pulse [55], hence protons are roughly four orders of magnitude more effective in causing SEE effects in fibers than neutrons. Although the atmospheric neutron flux is higher than that of the protons by less than an order of magnitude, as seen in Fig. 5, the protons are

nearly four orders of magnitude more effective than the neutrons in causing SEE effects in the fibers. Therefore, in terms of single event effects in fiber optic systems, it is the atmospheric protons that pose the main potential threat rather than atmospheric neutrons. In the same way that space systems successfully dealt with SEE effects in fiber optic systems once these potential effects were recognized [54,55], it is expected that such SEE effects can be similarly handled in avionics systems.

VII . SUMMARY AND CONCLUSIONS

Single event effects in avionics have been reviewed. Considerable attention was focused on the ionizing radiation environment in the atmosphere that causes the SEE, as well as the various sources of data that correlate the occurrence of SEE at aircraft altitudes with the atmospheric neutrons. Two different approaches were reviewed that have been successful in utilizing laboratory-generated SEU cross section data to calculate the upset rates at altitude. Information was provided on the simulation and testing of microelectronic devices for SEE effects for purposes of avionics applications, as well as on the other SEE effects besides upset that might be of concern in avionics. Systems impacts were not directly addressed. In general terms, error detection and correction (EDAC) and redundancy are the two system approaches most often used to avoid problems with SEE. These are more fully discussed in [2,3,8]. EDAC, which can defeat upsets in large memory arrays, is now being incorporated into a number of commercially available computer systems aimed at the avionics market, and this trend is likely to continue.

References

- 1) H. May, "A New Enemy-Homotrons", International Federation of Airline Pilots Association (IFALPA) Newsletter, September, 1980
- 2). A. Taber and E. Normand, "Single Event Upset in Avionics", IEEE Trans. Nucl. Sci., NS-40, 120, 1993
- 3) A. Taber and E. Normand, "Investigation and Characterization of SEU Effects and Hardening Strategies in Avionics", IBM Report 92-L75-020-2, August, 1992, republished as DNA-Report DNA-TR-94-123, Defense Nuclear Agency, Feb, 1995
- 4) D. F. Smart and M. A. Shea, "Cosmic Ray Exposure Factors for Shuttle Altitudes Derived from Calculated Cut-off Rigidities", Adv. Space Res., 4, No. 10, 161 (1984)
- 5) E. Normand and T. J. Baker, "Altitude and Latitude Variations in Avionics SEU and Atmospheric Neutron Flux", IEEE Trans. Nucl. Sci., 40, 1484 (1993)
- 6) J. Hewitt, L. Hughes, J. W. Baum, A. V. Kuehner, J. B. McCaslin, A. Rindi, A. R. Smith, L. D. Stephens, R. H. Thomas, R. V. Griffith and C. G. Welles", Ames Collaborative Study of Cosmic Ray Neutrons: Mid-Latitude Flights", Health Physics, 34, 375, 1978
- 7) O. C. Allkofer and P. K. Grieder, Physics Data: Cosmic Rays on Earth, Fachinformationszentrum Energie, Physik, Mathematik GmbH, Karlsruhe, 1984
- 8) E. Normand, "Single Event Effects in Systems Using Commercial Electronics in Harsh Environments", 1994 IEEE Nuclear and Space Radiation Effects Conference Short Course, Tucson, AZ, July, 1994
- 9) M. Merker, E. S. Light, H. J. Verschell, R. B. Mendell and S. A. Korff, "Time Dependent Worldwide Distribution of Atmospheric Neutrons and of Their Products. Part 1" J. Geophys. Res. 78, 2727 (1973)
- 10) J. W. Wilson, L. W. Townsend, W. Schimmerling, G. Khandelwal, F. Khan, J. E. Nealy, F. A. Cucinotta, L. C. Simonsen, J. L. Shinn and J. W. Norbury, "Radiation Safety in the Earth's Atmosphere", in NASA RP-1257, Transport Mehds and Interactions for Space Radiations, p. 519, December, 1991 [For corrections to some model coefficients see Ref. 5 above.]
- 11) H. B. Barber, T. Bown, D. A. DeLise, E. W. Jenkins, J. J. Jones, R. M. Kalbach and A. E. Pifer, "Predictions and Measurements of Mass Spectra of the Charged Nucleonic Component of Cosmic Rays at Mountain Altitude", Phys. Rev. D22, 2667 (1980)
- 12) F.B. McDonald and W. R. Webber, "Proton Component of the Primary Cosmic Radiation", Phys. Rev. 115, 194, (1959)

- 13) N. A. Bui Van, I. M. Martin, Y. I. Stozhkov, M. I. Fradkin and A. Svirzhevskaya, "Secondary Protons in the Atmosphere at Different Latitudes", Nuovo Cimento, 16, 179 (1993)
- 14) W. R. Webber and J.F. Ormes, "Cerenkov-Scintillation Measurements of Nuclei Heavier than Helium in the Primary Cosmic Radiation", J. Geophys. Res. 72, 5957 (1967)
- 15) F. Hajnal, "Measurements of Dose Rate by External Radiation During Commercial Air Flights - A Proposal", US DOE-EML, May, 1992
- 16) MIL-HDBK-781 Military Handbook - Reliability Test Methods, Plans and Environments for Engineering Development, Qualification and Production, USDoD, 1987
- 17) R. Silberberg, C. H. Tsao and J. R. Letaw, "Neutron Generated Single Event Upset in the Atmosphere", IEEE Trans. Nucl. Sci., NS-31, 1066 and 1183, Dec. 1984
- 18) J. Olsen, P. E. Becher, P. B. Fynbo, P. Raaby and J. Schultz, "Neutron-Induced Single Event Upsets in Static RAMs Observed at 10 Km Flight Altitude", IEEE Trans. Nucl. Sci., 40, 74, 1993
- 19) J. P. Raymond and C. P. Capps, "Aircraft SEU Phenomena", paper presented at the Eighth Single Event Effects Symposium, Los Angeles, April, 1992
- 20) J. Priborsky, personal communication
- 21) C. S. Dyer, A. J. Sims, J. Farren and J. Stephen, "Measurements of the SEU Environment in the Upper Atmosphere", IEEE Trans. Nucl. Sci., NS-36, 2275 (1989)
- 22) C. S. Dyer, A. J. Sims, J. Farren and J. Stephen, "Measurements of Solar Flare Enhancements to the Single Event Upset Environment in the Upper Atmosphere", IEEE Trans. Nucl. Sci., NS-37, 1929, 1990
- 23) E. Normand, D. L. Oberg, J. L. Wert, J. D. Ness, P. P. Majewski, S. A. Wender and A. Gavron, "Single Event Upset and Charge Collection Measurements Using High Energy Neutrons and Protons", IEEE Trans. Nucl. Sci., 41, 2203, 1994
- 24) T. Nakamura, Y. Uwamino, T. Ohkubo and A. Hara, "Altitude Variation of Cosmic Ray Neutrons", Health Physics, 53, 509 (1987)
- 25) T. O'Gorman, "An Experiment to Determine the Effect of Cosmic Rays on a FET Computer Memory", paper presented at the Fourth Single Event Effects Symposium, Los Angeles, 1985
- 26) T. O'Gorman, "The Effect of Cosmic Rays on the Soft Error Rate of a DRAM at Ground Level", IEEE Trans. Electron Devices, 41, 553 (1994)

- 27) M. Fischler, personal communication
- 28) C. Lage, D. Burnett, T. McNelly, K. Baker, A. Bormann, D. Dreier and V. Soorholtz, "Soft Error Rate and Stored Charge Requirements in Advanced High Density SRAMs", IEDM Tech. Digest, 821 (1993)
- 29) J. F. Dicello, M. Paciotti and M. E. Schillaci, "An Estimate of Error Rates in Integrated Circuits at Aircraft Altitudes and at Sea Level", Nucl. Inst. and Methods, B40, 1295 (1989)
- 30) E. Normand, D. L. Oberg, J. L. Wert, T. J. Baker and C. M. Castaneda, "Considerations in Single Event Upset Testing with Energetic Neutrons", paper presented at the Eighth Single Event Effects Symposium, Los Angeles, April, 1992
- 31) J. F. Ziegler and W. A. Lanford, "Effect of Cosmic Rays on Computer Memories", Science, 206, 776 (1979)
- 32) J. R. Letaw and E. Normand, "Guidelines for Predicting Single Event Upsets in Neutron Environments", IEEE Trans. Nucl. Sci., NS-38, 1500, 1991
- 33) J. R. Letaw, "Burst Generation Rates on Silicon and Gallium Arsenide from Neutron-Induced Recoils" SCC Report 87-02, Severn Communication Corp., 1987
- 34) E. Normand and W. R. Doherty, "Incorporation of ENDF-V Neutron Cross Section Data for Calculating Neutron-Induced Single Event Upsets", IEEE Trans. Nucl. Soc., NS-36, 2349 (1989)
- 35) E. L. Petersen, J. C. Pickel, J. H. Adams and E. C. Smith, "Rate Prediction for Single Event Effects" IEEE Trans. Nucl. Sci., 39, 1577 (1992) [see also follow-on paper, IEEE Trans. Nucl. Sci., 40, 1888, (1993)]
- 36) P. J. McNulty, W. J. Beauvais and D. R. Roth, Determination of SEU Parameters of NMOS and CMOS SRAMs", IEEE Trans. Nucl. Soc., NS-38, 1463 (1991)
- 37) E. Normand, "Calculating Proton-Induced SEU Using Heavy Ion Data Via the Burst Generation Rate Method", Boeing Internal Report, 1995
- 38) A. J. Sims, C. S. Dyer, C. L. Peerless, K. Johansson, H. Pettersson and J. Farren, "The Single Event Upset Environment for Avionics at High Latitude", IEEE Trans. Nucl. Sci., 41, 2361, (1994)
- 39) P. Lisowski et al "The Los Alamos National Laboratory Spallation Neutron Sources" Nucl. Sci. Eng., 106, 208 (1990)
- 40) A. M. Hofert and G. Stevenson, "The CERN-CEC High-Energy Reference Field Facility", Proceedings of the 8th International Conference on Radiation Shielding, Arlington, TX, April, 1994, p. 635

- 41) L. E. Moritz, "Measurement of Neutron Leakage Spectra at a 500 MeV Proton Accelerator", Health Physics, 56, 287, 1989
- 42) F. Spurny, I. Votockova and V. P. Bamblevski, "On the Energy Dependence of Bubble Damage Neutron Detectors", Nucl. Tracks Radiat. Meas., 23, 251, (1994)
- 43) "Neutron Testing and Analysis of the LSI Logic LCA 100K/200K Gate Array", Honeywell report C71-5810-004, Feb. 1993
- 44) E. Normand, J. L. Wert, D. L. Oberg, P. P. Majewski, W. G. Bartholet, S. K. Davis, M. Shoga, S. A. Wender and A. Gavron, "Single Event Upset and Latchup Measurements in Avionics Devices Using the WNR Neutron Beam and a New Neutron-Induced Latchup Model", Workshop Record, 1995 IEEE Radiation Effects Data Workshop, p. 33
- 45) L. Adams, E. J. Daly, R. Harboe-Sorensen, R. Nickson, J. Haines, W. Schafer, M. Conrad, H. Griech, J. Merkel, T. Schwall and R. Henneck, "A Verified Proton Induced Latchup in Space", IEEE Trans. Nucl. Sci., 39, 1804 (1992)
- 46) D. Nichols, J. R. Coss, R. K. Watson, H. R. Schwartz and R. L. Pease, "An Observation of Proton-Induced Latchup", IEEE Trans. Nucl. Sci., 39, 1654 (1992)
- 47) J. Levinson, A. Akkerman, M. Victoria, M. Haas, D. Ilberg, M. Alurralde, R. Henneck, and Y. Lifshitz, "New Insights Into Proton Induced Latchup: Experiment and Modeling", Appl. Phys. Letters, 63(21), 22, Nov. 1993
- 48) D. L. Schaeffer, J. R. Kimbrough, J. W. Wilburn, S. M. Denton, J. L. Kaschmitter, N. J. Colella, P. G. Coakley and C. Castaneda, "Proton-Induced SEU, Dose Effects, and LEO Performance Predictions for R3000 Microprocessors", IEEE Trans. Nucl. Sci., 39, 2309 (1992)
- 49) J. L. Titus, L. S. Jamiolkowski and C. F. Wheatley, "Development of Cosmic Ray Hardened Power MOSFETs" IEEE Trans. Nucl. Sci., 36, 2375, (1989)
- 50) A. E. Waskiewicz and J. W. Groninger, "Burnout Threshold and Cross Sections of Power MOS Transistors with Heavy Ions", Rockwell International Report DNA-MIPR-88-507 (1990)
- 51) D. L. Oberg and J. L. Wert, personal communication
- 52) D. L. Oberg and J. L. Wert, "First Nondestructive Measurements of Power MOSFET Single Event Burnout Cross Sections", IEEE Trans. Nucl. Sci., 34, 1736, (1987)
- 53) D. K. Nichols, K. P. McCarty, J. R. Coss, A. Waskiewicz, J. Groninger, D. L. Oberg, J. L. Wert, P. P. Majewski and R. Koga, "Observations of Single Event Failure in Power MOSFETs", Workshop Record, 1994 IEEE Radiation Effects Data Workshop, 1994

- 54) P. W. Marshall, C. J. Dale and E. A. Burke, "Physical Interactions Between Charged Particles and Optoelectronic Devices and Their Effects on Fiber Optic Data Links" Proc. SPIE, 53, 104 (1993)
- 55) P. W. Marshall, C. J. Dale, E. J. Friebele and K. A. LaBel, "Survivable Fiber Based Data Links for Satellite Radiation Environments" SPIE Critical Review, 1993
- 56) P. W. Marshall, C. J. Dale and E. A. Burke, IEEE Trans. Nucl. Sci., 39, 1982 (1992)
- 57) E. Normand, D. L. Oberg, J. L. Wert, P. P. Majewski, G. A. Woffinden, S. Satoh, K. Sasaki, M. G. Tverskoy, V. V. Miroshkin, N. Goleminov, S. A. Wender and A. Gavron, "Comparison of Charge Collection Measurements in Silicon and InGaAs Irradiated by Energetic Protons and Neutrons", paper presented at the 1995 IEEE NSREC Meeting, Madison, WI, July, 1995

FIGURE CAPTIONS

Figure 1 Spectrum of the average differential neutron flux in the atmosphere at 40,000 ft. and 45° latitude based on the measurements of NASA-Ames and normalized to a 1-10 MeV neutron flux of 0.85 n/cm² sec [2,3].

Figure 2 The 1-10 MeV atmospheric neutron flux as a function of altitude based on aircraft and balloon measurements [2].

Figure 3 The 1-10 MeV neutron flux as a function of geographical latitude based on aircraft neutron measurements and the vertical rigidity cutoffs of Smart and Shea [4,5].

Figure 4 Comparison of Measured Atmospheric Proton Spectra at Several Altitudes [7,11]

Figure 5 Comparison of Measured Atmospheric Proton Flux (100<E<750 MeV) As Function of Atmospheric Depth [11,12]

Figure 6 Falloff of Vertical Ion Flux with Atmospheric Depth at the Top of the Atmosphere For Ions of Energy >200 MeV/nucl. [14]

Figure 7 Correlation of the inflight SEU rate in the IMS 1601 SRAM with atmospheric neutron flux as a function of altitude. The SRAM was operated at 2.5V [2].

Figure 8 Correlation of the inflight SEU rate in the IMS 1601 SRAM with atmospheric neutron flux as a function of geographical latitude. The SRAM was operated at 5V [5].

Figure 9 Correlation of the energy deposition spectrum in the CREAM detector flown on Concorde with spectra measured in silicon surface barrier detectors in the WNR beam. [21-23]

Figure 10 Comparison of the neutron spectrum at the Weapons Neutron Research facility (WNR) of Los Alamos National Lab with the atmospheric neutron spectrum [23].

FIGURE CAPTIONS

Figure 1 Spectrum of the average differential neutron flux in the atmosphere at 40,000 ft. and 45° latitude based on the measurements of NASA-Ames and normalized to a 1-10 MeV neutron flux of 0.85 n/cm² sec [2,3].

Figure 2 The 1-10 MeV atmospheric neutron flux as a function of altitude based on aircraft and balloon measurements [2].

Figure 3 The 1-10 MeV neutron flux as a function of geographical latitude based on aircraft neutron measurements and the vertical rigidity cutoffs of Smart and Shea [4,5].

Figure 4 Comparison of Measured Atmospheric Proton Spectra at Several Altitudes [7,11]

Figure 5 Comparison of Measured Atmospheric Proton Flux (100<E<750 MeV) As Function of Atmospheric Depth [11,12]

Figure 6 Falloff of Vertical Ion Flux with Atmospheric Depth at the Top of the Atmosphere For Ions of Energy >200 MeV/nucl. [14]

Figure 7 Correlation of the inflight SEU rate in the IMS 1601 SRAM with atmospheric neutron flux as a function of altitude. The SRAM was operated at 2.5V [2].

Figure 8 Correlation of the inflight SEU rate in the IMS 1601 SRAM with atmospheric neutron flux as a function of geographical latitude. The SRAM was operated at 5V [5].

Figure 9 Correlation of the energy deposition spectrum in the CREAM detector flown on Concorde with spectra measured in silicon surface barrier detectors in the WNR beam. [21-23]

Figure 10 Comparison of the neutron spectrum at the Weapons Neutron Research facility (WNR) of Los Alamos National Lab with the atmospheric neutron spectrum [23].

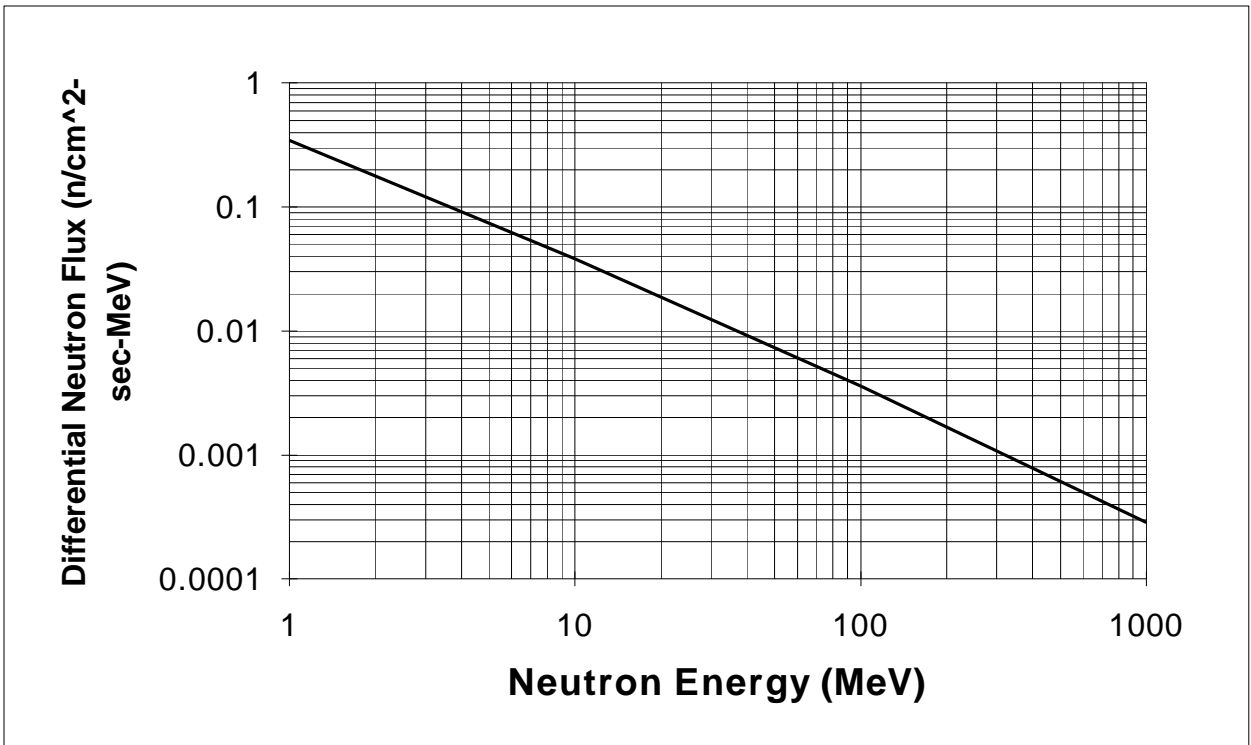


Figure 1 Spectrum of the average differential neutron flux in the atmosphere at 40,000 ft. and 45° latitude based on the measurements of NASA-Ames and normalized to a 1-10 MeV neutron flux of 0.85 n/cm² sec [2,3].

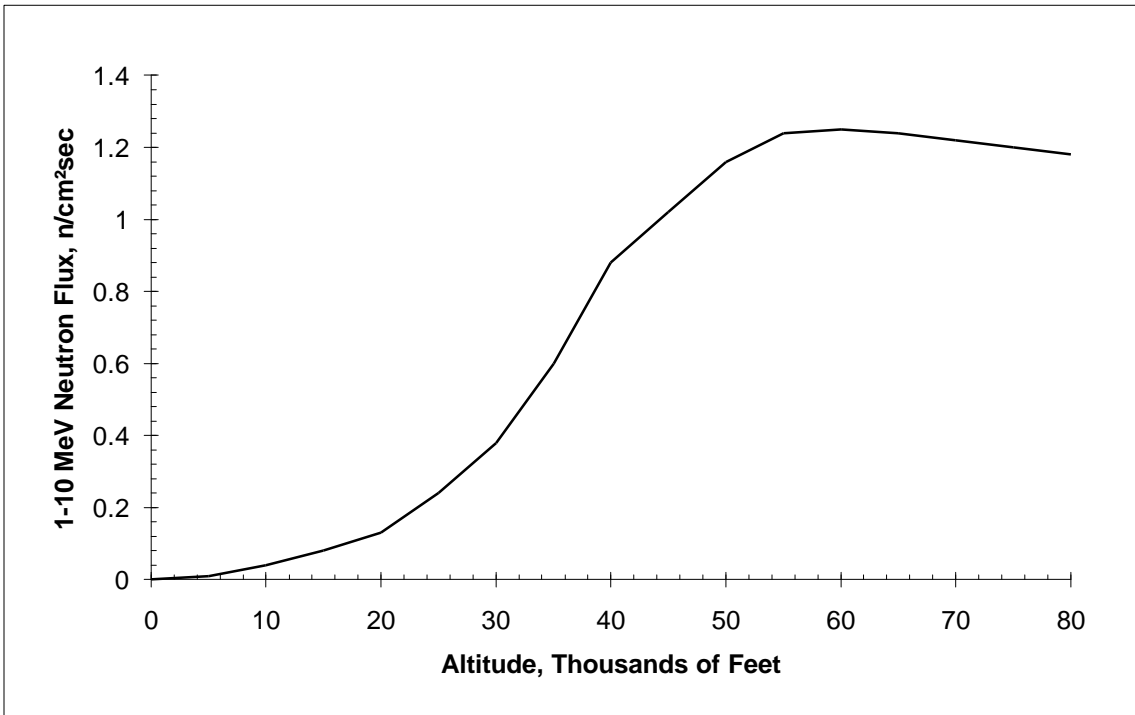


Figure 2 The 1-10 MeV atmospheric neutron flux as a function of altitude based on aircraft and balloon measurements [2].

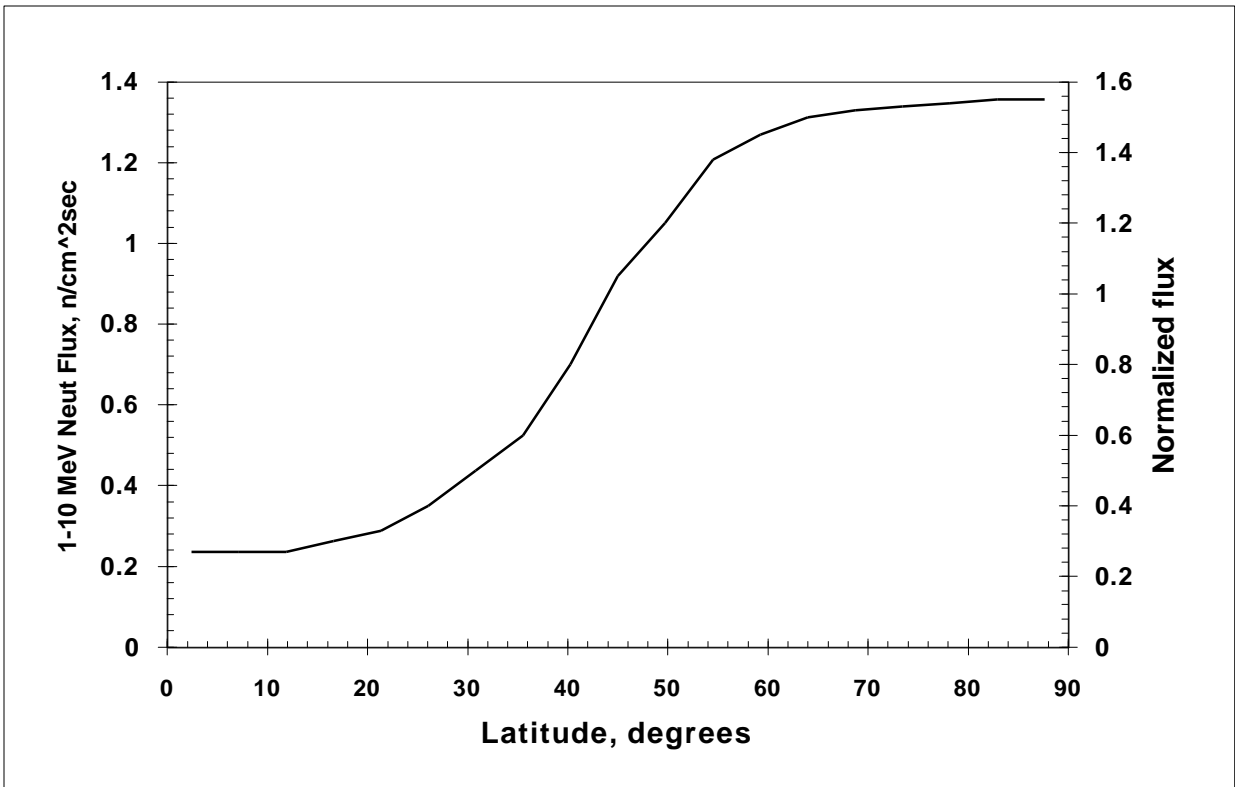


Figure 3 The 1-10 MeV neutron flux as a function of geographical latitude based on aircraft neutron measurements and the vertical rigidity cutoffs of Smart and Shea [7,9].

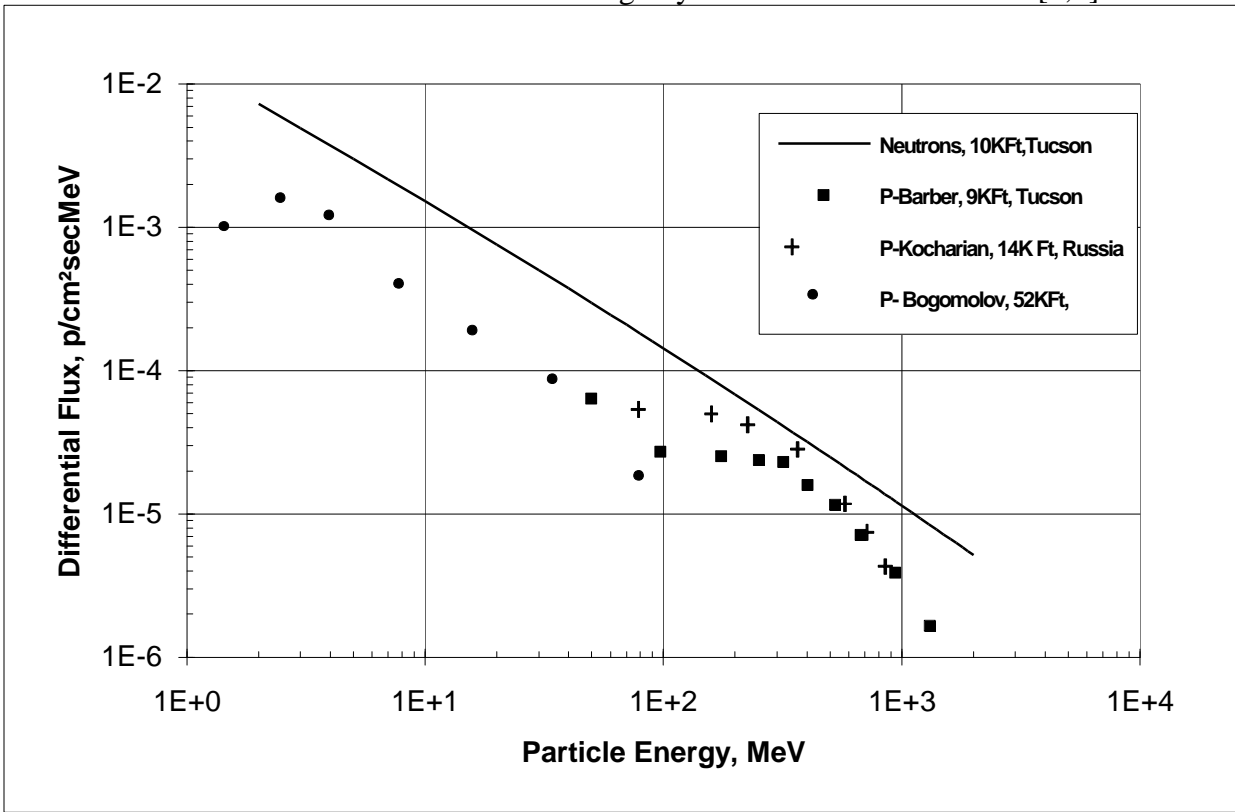


Figure 4 Comparison of Measured Atmospheric Proton Spectra at Several Altitudes [6,10]

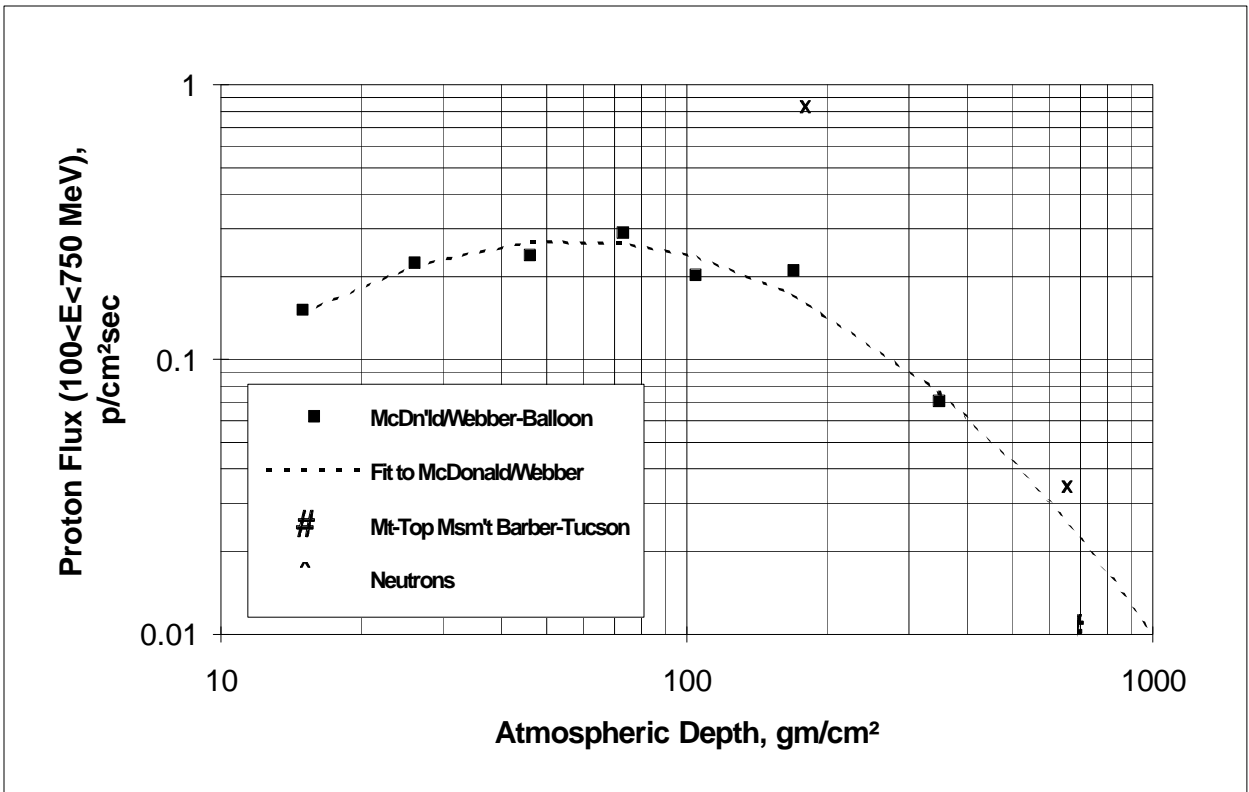


Figure 5 Comparison of Measured Atmospheric Proton Flux (100<E<750 MeV) As Function of Atmospheric Depth [9,10]

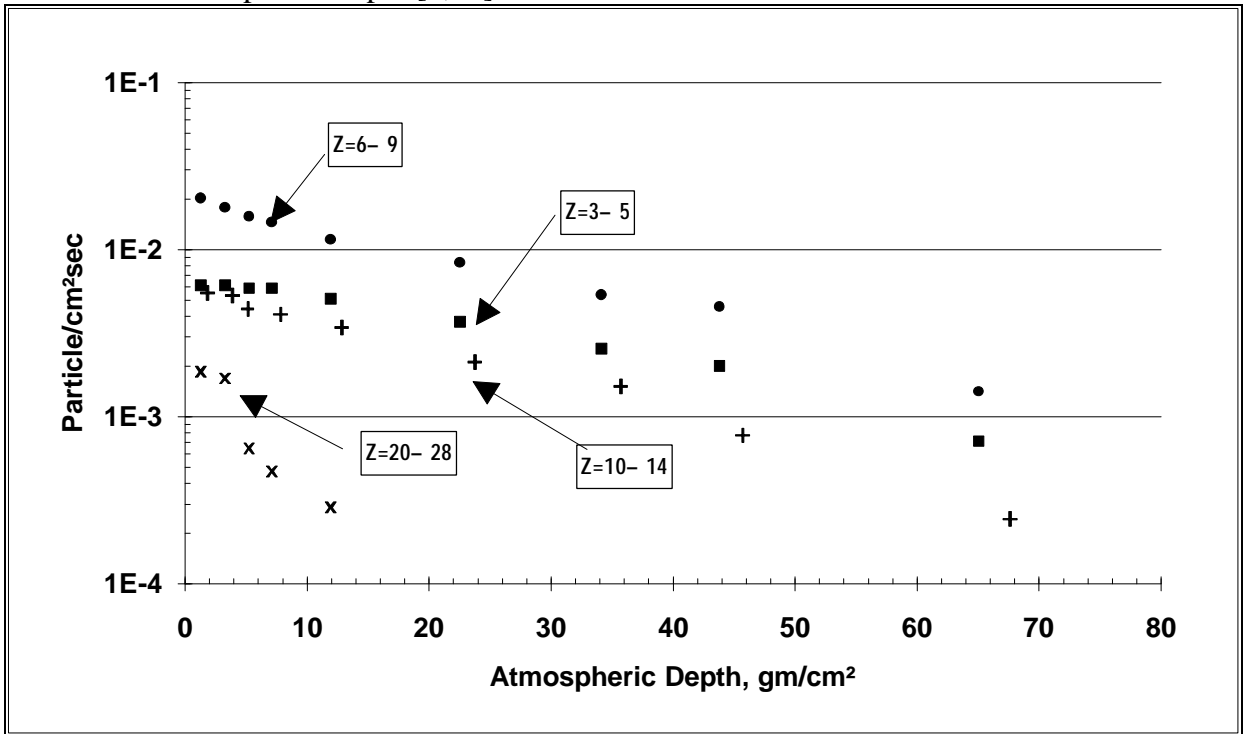


Figure 6 Falloff of Vertical Ion Flux with Atmospheric Depth at the Top of the Atmosphere For Ions of Energy >200 MeV/nucl. [53]

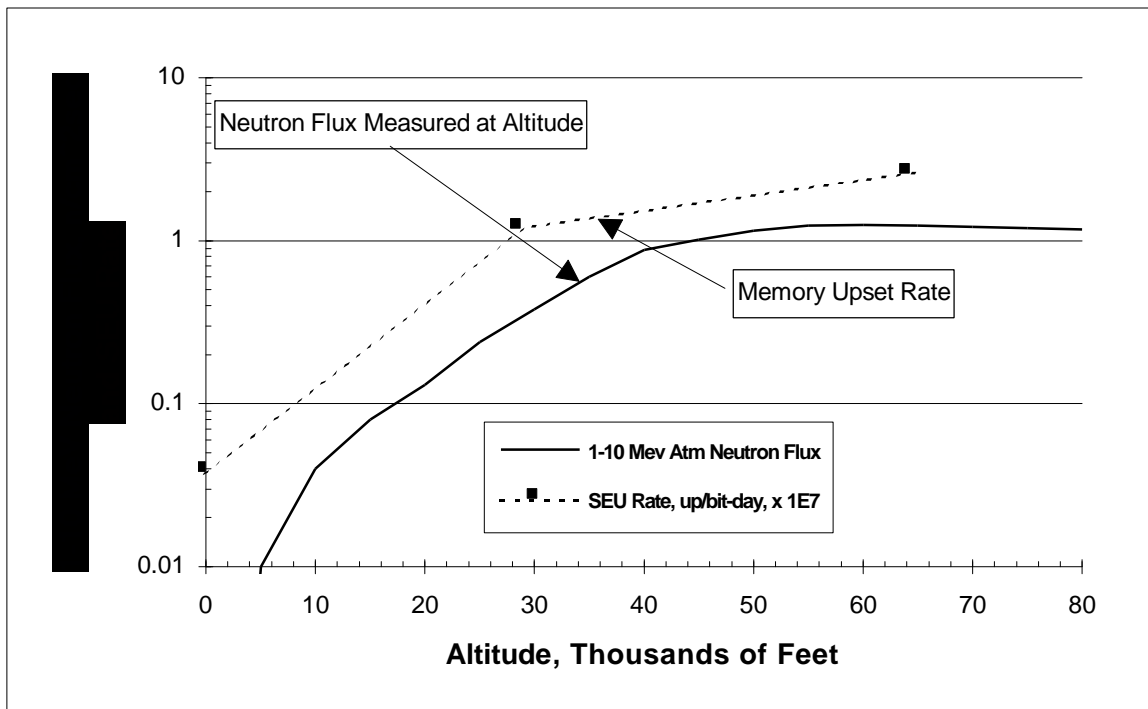


Figure 7 Correlation of the in-flight SEU rate in the IMS 1601 SRAM with atmospheric neutron flux as a function of altitude. The SRAM was operated at 2.5V [2].

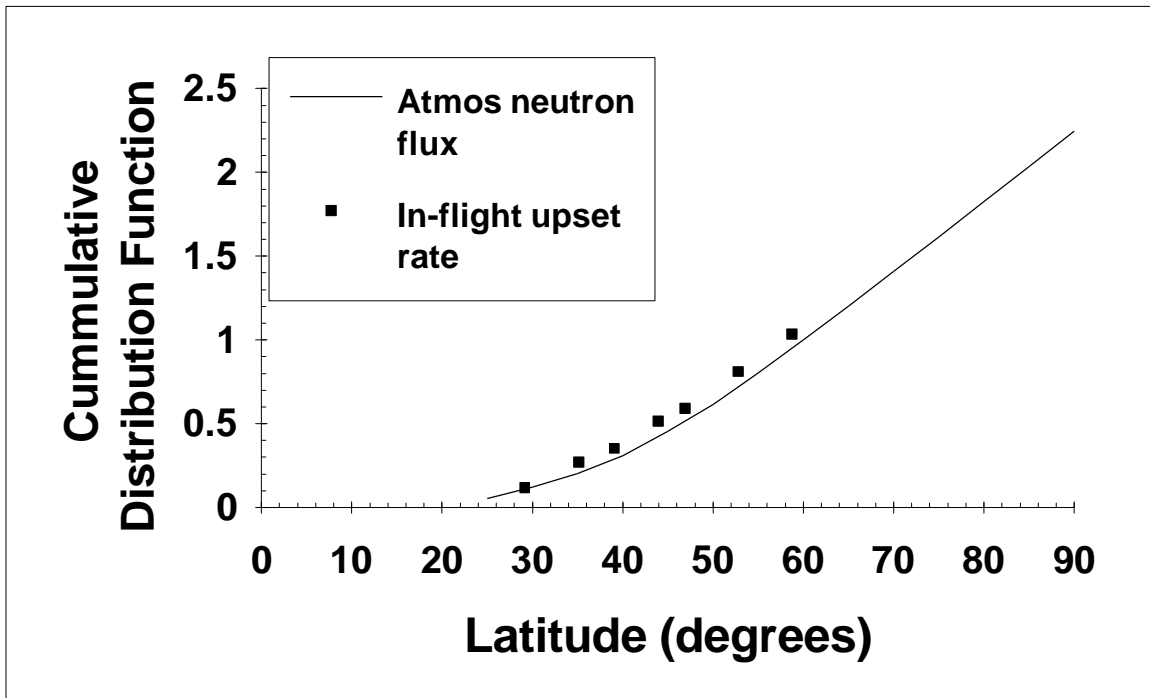


Figure 8. Correlation of the in-flight SEU rate in the IMS 1601 SRAM with atmospheric neutron flux as a function of geographical latitude. The SRAM was operated at 5V [7].

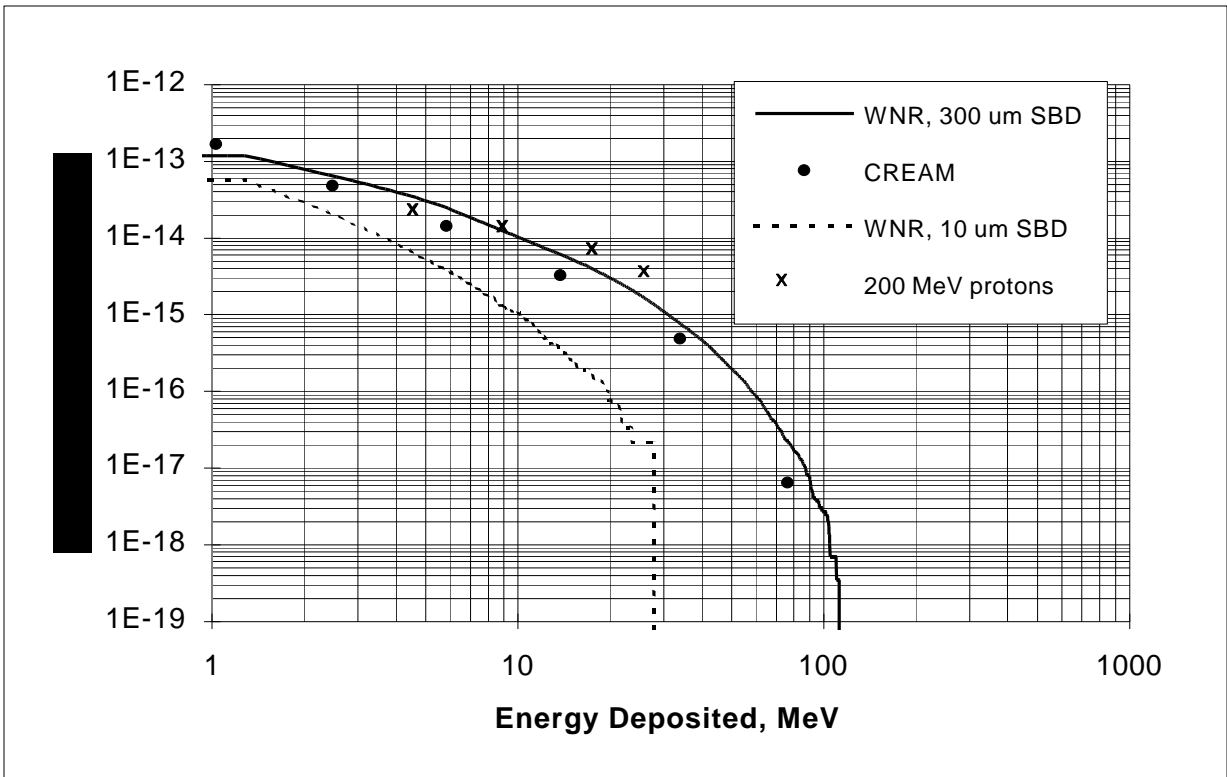


Figure 9 Correlation of the energy deposition spectrum in the CREAM detector aboard Concorde with spectra measured in silicon surface barrier detectors in the WNR beam. [17-19].

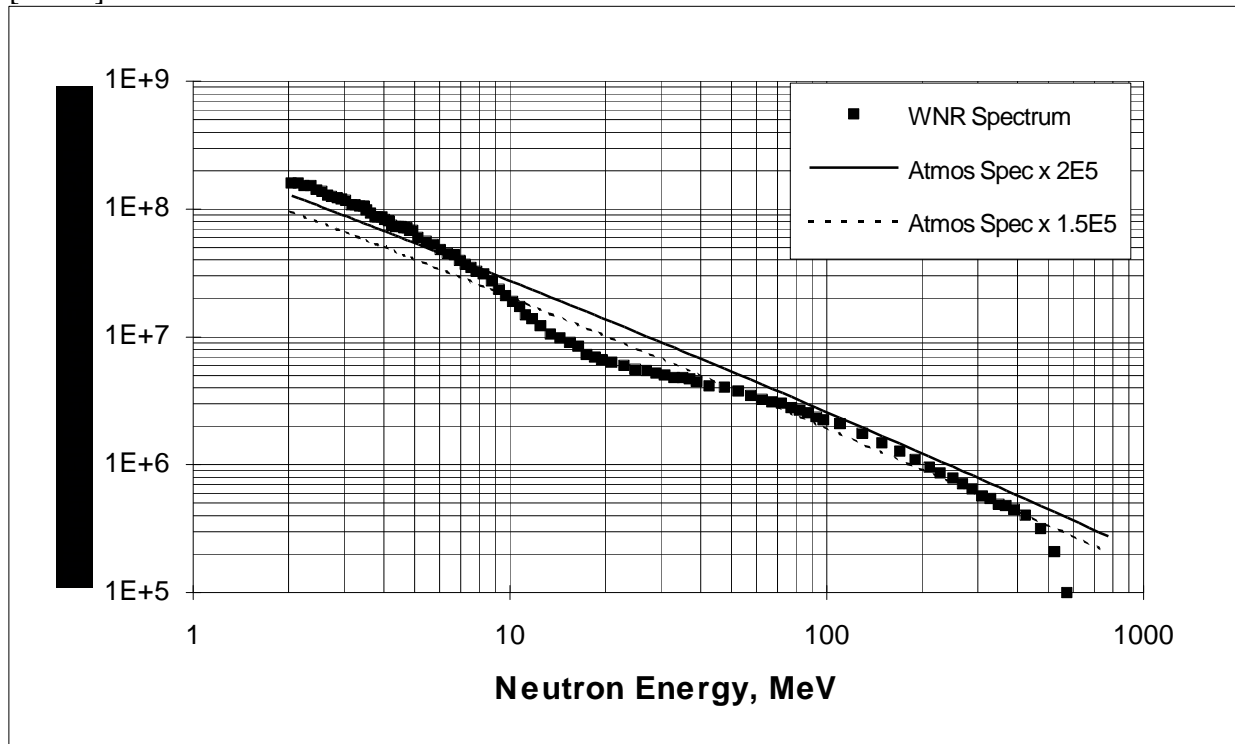


Figure 10 Comparison of the neutron spectrum at the Weapons Neutron Research facility (WNR) of Los Alamos National Lab with the atmospheric neutron spectrum [19].

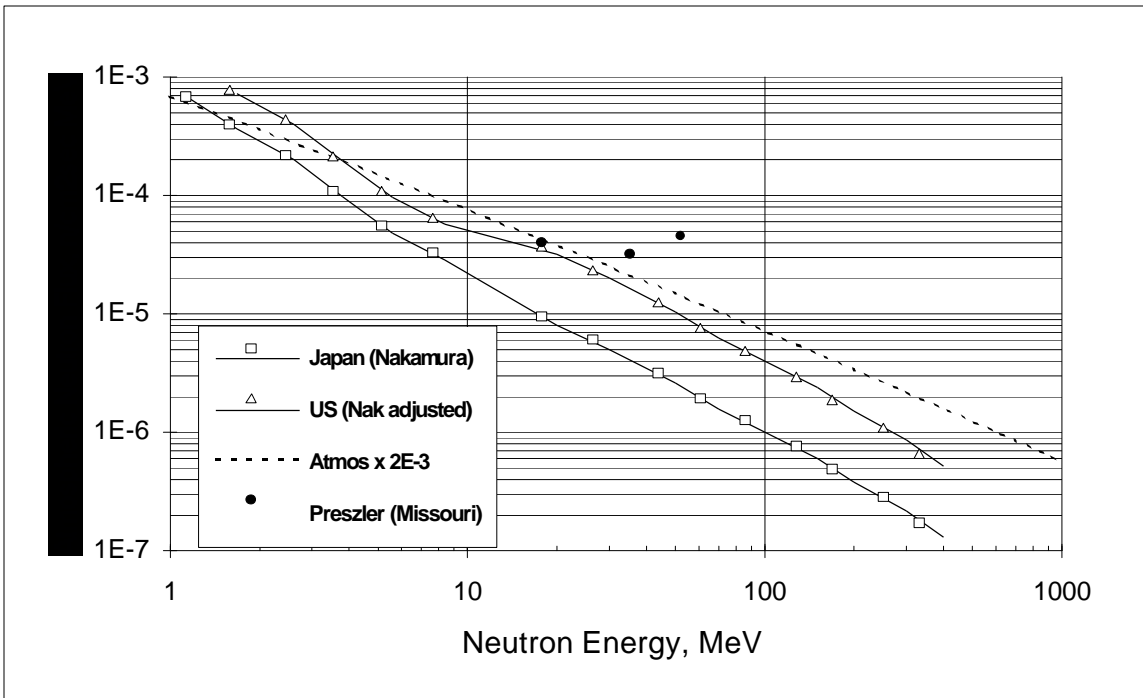


Figure 13 Comparison of ground-level atmospheric neutron spectra with the spectrum of neutrons at 40,000 ft. [118, 136].

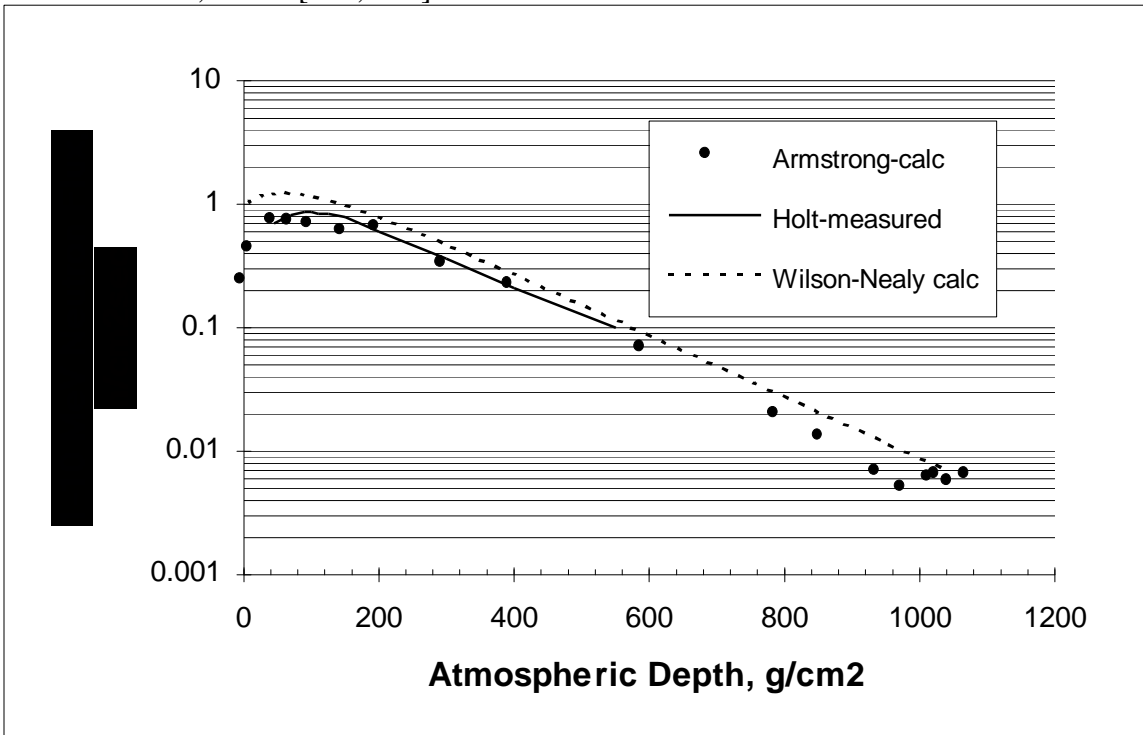


Figure 3. The 1-10 MeV atmospheric neutron flux as a function of atmospheric depth (g/cm^2) based on balloon measurements (Holt) and calculations (Armstrong and Wilson-Nealy) [33, 35]